Astronomy
&
Astrophysics

Surface density of extremely red objects with $R - J \geq 5$

A. Hempel[1,2], T. M. Herbst[2], and D. J. Thompson[2,3]

[1] Geneva Observatory, 51 Ch. des Maillettes, Sauverny 1290, Switzerland
  e-mail: Angela.Hempel@obs.unige.ch
[2] Max Planck Institute for Astronomy (MPIA), Königstuhl 17, 69117 Heidelberg, Germany
  e-mail: herbst@mpia.de
[3] The Palomar Observatory, California Institute of Technology, Pasadena, CA 91125, USA
  e-mail: djt@irastro.caltech.edu

ABSTRACT

We present the results of a wide-field survey for extremely red objects (EROs), based on J and R band imaging. The survey covers 2.89 deg^2, consisting of 50 single fields, each approximately 210 arcmin^2 in size. This survey provides a sample of 60 extended objects with a colour of $R - J \geq 5$ and J band magnitudes more than 10σ above background ($18^{mag} \leq J \leq 20^{mag}$).
Thirty five of these objects have been detected in both J and R-band. We derive a surface density for such EROs of $5.7 \pm 0.1 \times 10^{-3}$ arcmin^{-2}, which is about seven times lower than for galaxies with $R - K \geq 6$.
Stellar population models suggest that these EROs are massive galaxies with an old stellar population in a redshift range of $1.4 \leq z \leq 3.0$. For this scenario, we estimate the co-moving volume density to be $(9.57 \pm 1.24) \times 10^{-6}$ Mpc^{-3}.

Key words. Galaxy: evolution – galaxies: high-redshift – galaxies: elliptical and lenticular, cD

1. Introduction

Extremely red objects (EROs), discovered in deep optical and near-infrared surveys, are proving to be a heterogeneous population. Defined mostly by a single colour, usually $R - K$, the ERO population contains substellar objects, cool stars, galaxies, and active galactic nuclei. Galaxies may appear very red because of extreme redshifts, old populations at intermediate redshifts, or severe dust reddening (or combinations of these factors). The very red optical-to-near-infrared colour covers a wide range ($R - K \gtrsim 5 - 7$ or $I - K \gtrsim 4 - 6$), hence allowing various interpretations regarding their nature. First detections of EROs were initially presumed to be high-redshift ($z > 6$) galaxies in a luminous star-forming phase (Elston et al. 1988). Multi-colour follow-up observations identified these objects as luminous galaxies at $z = 0.8$, dominated by an old stellar population (Elston et al. 1989). The detection of HR10 and HR14, two bright ($K \geq 18.5$) extended objects with $I - K$ colours near 6.5 by Hu & Ridgway (1994) gave an indication of the difficulties in classifying these objects. When first discovered, HR10 and HR14 were interpreted as being ellipticals at $z \sim 2.4$. Subsequent spectroscopic and morphological observations indicated that HR10 is not a quiescent elliptical galaxy, but rather a bright interacting galaxy at $z = 1.44$ (Graham & Dey 1996).

Additional EROs, both massive old and dusty interacting galaxies, were found by various groups (e.g. Cowie et al. 1994; Soifer et al. 1999; Thompson et al. 1999; McCracken et al. 2000; Afonso et al. 2001; Cimatti et al. 2002a). These objects appeared in the field of quasars (Liu et al. 2000; Hall et al. 2001; Smith et al. 2002a), as counterparts of sub-millimeter galaxies (Smail et al. 1999; Mohan et al. 2002), and in dedicated surveys (Daddi et al. 2002; Cimatti et al. 2002a,b).

Strategies to distinguish the fraction of different extragalactic ERO types include near-infrared photometric classification (Pozzetti & Mannucci 2000; Mannucci et al. 2002; Martini 2001; Hempel et al. 2003), morphological tests (Yan et al. 2000; Yan & Thompson 2003; Gilbank et al. 2003; Moriondo et al. 2000), and an increasing number of spectroscopic discriminators (Cimatti et al. 1999, 2002a; Smith et al. 2001). Near-infrared spectroscopy of 9 EROs ($R - K > 5$ and $K < 19.0$) by Cimatti et al. (1999) showed neither strong emission lines nor continuum breaks. Two of their observed EROs were classified as dusty starburst candidates, because they require strong dust reddening to produce the observed global spectral energy distributions. The remaining ∼2/3 of the total ERO sample is consistent with being dustless, old, passively evolved, spheroidals at $z \gtrsim 0.8$. A larger sample of 30 EROs with $K \leq 19.2$ showed an almost equal distribution between old and star forming galaxies (Cimatti et al. 2002a). Based on the classification method of Pozzetti & Mannucci (2000), and using the $(R - K)$ vs. $(J - K)$ colour plane, Mannucci et al. (2002) also found an equal distribution of elliptical and starburst galaxies.

Morphological observations, based on optical and near-infrared HST data, allow a more detailed classification. Yan & Thompson (2003) visually classified both pure bulge or

disk galaxies and bulge or disk-dominated galaxies, using HST/WFPC2 *F814W* and groundbased K_s-band images of 115 EROs. They found that $30\pm5\%$ of the ($F814W-K_s \geq 4$) selected sample have morphologies consistent with a pure-bulge dominated galaxy (E/S0), while $64 \pm 7\%$ of the sample can be described as disks. A small fraction, 6%, could not be classified unambiguously. In addition, a significant fraction of edge-on spirals was detected: 40% of the disks, or 28% of the total sample, were of this type. Similar relative fractions of early and late type galaxies were found among a sample of 275 EROs ($R - K \geq 5$), detected in the Great Observatories Origins Deep Survey-South (GOODS-South) (Moustakas et al. 2004). Optical spectroscopy on a sub-sample of 36 sources (Yan et al. 2004) revealed a more complicated relation between spectral class and morphological appearance.

Hard X-ray observations are especially useful for detecting AGNs among the ERO population. Between ten and thirty percent of hard X-ray sources could be associated with EROs, depending on the limiting fluxes reached in the optical and the X-ray band (Brusa et al. 2002). The fraction of AGN among the optically detected EROs is still unclear, but possibly below 15%, suggesting that the majority of EROs are not related to AGN phenomena. A similarly low fraction of EROs has been found in the soft X-ray band, indicating either a low-luminosity AGN or starburst activity (Alexander et al. 2002; Brusa 2003). EROs, especially the dusty starburst population, contribute significantly to the 850 μm background (Wehner et al. 2002), pointing to a connection with sub-millimeter galaxies (SMG). Their near-infrared colour ranges from $J - K = 2$ for bright sources ($K < 19$) to extremely red ($J - K = 3$) for fainter SMG (Frayer et al. 2004).

The variety of colour criteria used to define EROs, for example $R - K \geq 5$, 5.3 or 6, the different survey depths, and the apparent strong clustering (Daddi et al. 2000; Roche et al. 2002, 2003), result in a wide range of surface densities (e.g. Hu & Ridgway 1994; Thompson et al. 1999; Yan et al. 2000). Recent and larger surveys suggest that the surface density of $R - K \gtrsim 6.0$ galaxies ($K \leq 19$) is 0.07 ± 0.012 arcmin^{-2}, increasing to 0.1 ± 0.01 at $K_s \leq 19.2$ (Daddi et al. 2000). For EROs with $R - K_s \gtrsim 7.0$ and brighter than $K_s = 19.2$, Daddi et al. (2000) derived a surface density of ~0.011 arcmin^{-2}.

The determination of the nature of EROs and their density is important, since EROs provide valuable clues to massive structure formation on large scales. In the CDM-based galaxy formation models, massive objects form through mergers and accretion. The number density of such massive structures at high redshifts can be used to test these models, by comparing their predictions with the observed number densities. Although hierarchical models reproduce the global star formation quite well (Bell et al. 2004; Roche et al. 2002), they have difficulties reproducing the observed number of extremely red objects, both quiescent ellipticals and dust-obscured star forming galaxies (Firth et al. 2002; Somerville et al. 2001; Cimatti et al. 2002b; Im et al. 2002a).

The main goal of our survey is to obtain a sample of ERO candidates with an extremely red colour of $R - J \geq 5$ and relatively bright J magnitudes ($J < 20^{\mathrm{mag}}$), suitable for spectroscopic follow-up. Clearly, the available data allow also the

application of less strict colour criteria, which will be subject in a forthcoming paper. This colour limit is considerably redder than the $R - K \geq 5$, 5.3 or 6 criterion assumed for most ERO surveys (Cimatti et al. 2002a; Roche et al. 2002), and selects a different galaxy population. In Sect. 3.1 we investigate how the star formation history can redden the spectral energy distribution of a galaxy sufficiently to classify them as ERO ($R - J \geq 5$).

In covering a larger area, we minimize the influence of clustering on the mean surface density of EROs, possibly measure the clustering itself, and provide targets for thorough spectroscopic follow-up. The total survey area is more than one order of magnitude larger than all previous ERO surveys (Daddi et al. 2000; Thompson et al. 1999; Roche et al. 2002). The only comparable ERO sample (see Sect. 3.1), using a colour threshold of $R - K \geq 7$ (Daddi et al. 2002), covers only 701 arcmin^2, and shows large statistical uncertainties.

Throughout this paper, a cosmology with $H_0 = 70$ km s^{-1} Mpc^{-1}, $\Omega_M = 0.3$ and $\Omega_\Lambda = 0.7$ is assumed.

2. Observations, data reduction and photometry

2.1. J-band imaging

The J-band data were taken during observing runs in October 1997, October 1998 and May 1999 with the 3.5 m telescope on Calar Alto. The observations were carried out using the prime focus camera Omega-Prime (Bizenberger et al. 1998), equipped with a 1024×1024 pixel HAWAII array. The pixel scale of 0.''3961/pixel gave a field of about $6.'78 \times 6.'78$. The J-band filter, centered at $\lambda_C = 1.275\ \mu$m and with a bandwidth of $\Delta\lambda = 0.290\ \mu$m was used. Each survey field was covered by a mosaic of 4 pointings, each consisting of 4 exposures of 60 s with small angular offsets. Herbst et al. (1999) provide further details on the observations.

The images were dark- and sky-subtracted using a sky-image constructed from science exposures taken close in time. Each image was then flat-fielded and cosmic rays and bad pixels were removed. The final images are 2300×2300 pixels, i.e. approximately (15×15) arcmin^2. Figure 1 contains an example field and indicates the depth of exposure. Adding up the usable area of all 50 fields results in a total survey area of ~2.89 degree^2.

The photometric zero-points were measured using the standard stars from the UKIRT catalogue observed at similar airmass. The effective image quality of the final mosaics ranges from about 1'' to 2.''1.

2.2. R-band imaging

The R-band observations were made by the *High-z Supernova Search Team Cosmology Project* with the 4.0 m Blanco telescope at the Cerro Tololo Inter-American Observatory (CTIO) during observing runs in 1994 through 1996 (Schmidt et al. 1998). The Prime Focus CCD Direct camera (PFCCD) was equipped with a 2048×2048 pixel array with 0.''40/pixel.

The observed fields span a wide range of right ascension, and consist of both clustered (Fig. 2) and isolated pointings.

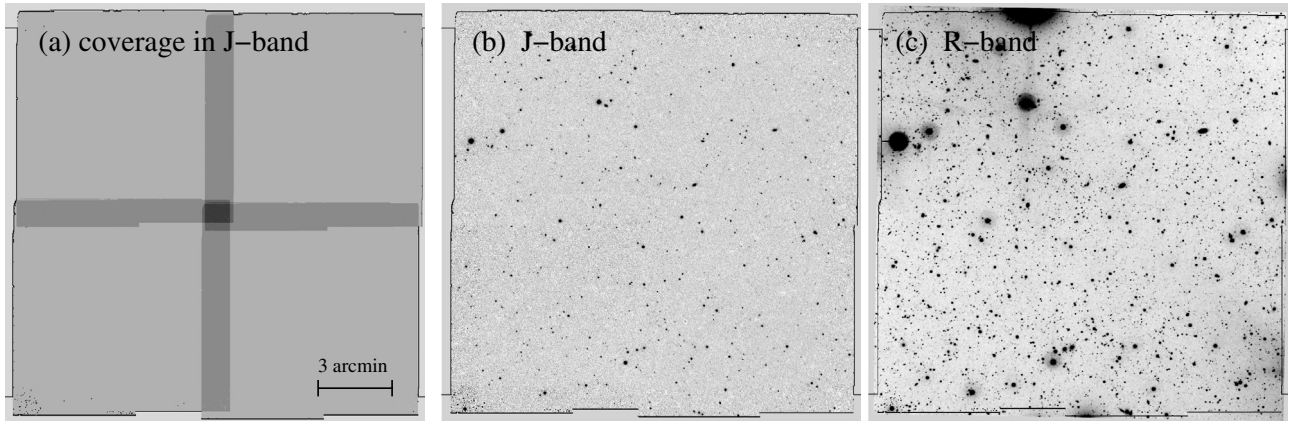**Fig. 1. a)** Gray-scale image showing the depth of a 2300×2300 pixel J-band mosaic. The lighter regions indicate higher noise due to a smaller number of exposures or bad pixels. Each sky position is measured at least 4 times. The rightmost two frames show a typical field in J- and R-band. The black line encloses the usable region (**b**) and **c**) respectively).
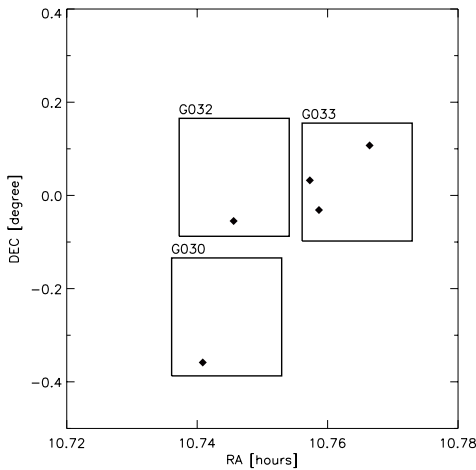

Fig. 2. Distribution on the sky of 3 survey fields, with a field size of about (15×15) arcmin^2. The symbols identify the detected EROs ($R - J \geq 5$). Fields are named by the letter G, followed by a three digit sequence number.

Fig. 3. The R-band zero point calibration for a typical field, based on Sloan Digital Sky Survey magnitudes. After correcting the assumed zero point, our photometry agrees very well with the SDSS results (standard deviation $\leq \pm 0.006$ mag).

Table 1. Transformation between $g' - r'$ and $V - R_C$.

V	$=$	$g' - 0.55(g' - r') - 0.03$
$V - R_C$	$=$	$0.59(g' - r') + 0.11$
R_C	$=$	$-0.14g' + 1.14r' + 0.14$

In order to minimize stellar contamination, we selected fields at high galactic latitudes, i.e $22° \leq |b| \leq 60°$. The fields are equatorial, and therefore accessible from observing sites in both the northern and southern hemispheres.

The total R-band exposure time varies from field to field, since evidence of supernovae resulted in additional observations, and hence longer integration times, for some locations. The slightly different pixel scale, a positional offset and a different orientation between the R and J-band image was compensated by adjusting the R-band images.

Since the available R-band data set did not include standard star observations, we used the Sloan Digital Sky Survey for calibration. We constructed a catalogue of un-saturated stars (between 50–80 stars per field, depending on image depth) and compared their R-band magnitudes with SDSS photometry (Fig. 3). For the transformation between R_C (R-Cousins filter) and the Sloan system we used the equations from Smith et al. (2002b) (see Table 1): the data were calibrated to match the transformed SDSS magnitudes, and R-band magnitudes were calculated for all near-infrared sources. The transformation equations were derived from the $u'g'r'i'z'$ photometry of
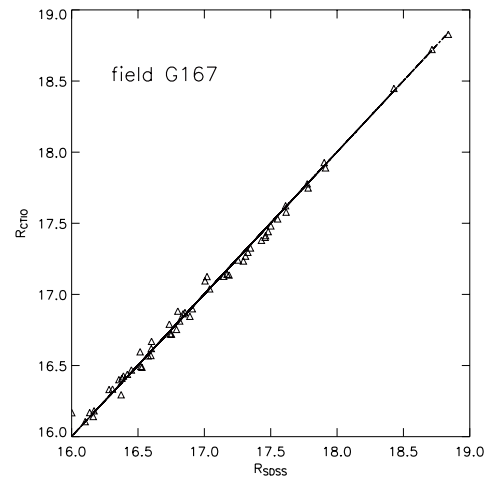
158 standard stars. The uncertainty in the mean calibrated magnitudes for any given standard star should be less than 1% in g' and r', resulting in a error of less than 0.02 mag in $g' - r'$.

2.3. Sample selection and photometry

Sources were first identified in the near-infrared data using SExtractor 2.2.2 (Bertin & Arnouts 1996), with the criterion that a source must exceed 5σ above the background in at least 5 pixels. The photometry is based on the SExtractor "BEST"-magnitude and refers to Vega magnitudes. Photometry in the R-band was then obtained by running SExtractor in 'double-image' mode, using the source position in the J-band

image to measure the R-band fluxes. The number of sources and their positions are therefore given by the J-band. On average, each field contains approximately 600 stellar or extragalactic objects with J-band detections. Objects closer than 3 pixels from the borders of the effective area (Fig. 1) were excluded from the initial catalogue. Although our selected fields are at relatively high galactic latitude, the frames inevitably contain stellar objects. To separate galaxies from stars, we used the stellarity index (CLASS_STAR parameter), provided by SExtractor. This star/galaxy classifier uses a total of 10 parameters (8 isophotal areas, peak intensity and 1 control parameter, which is the seeing) to identify stars (stellarity index = 1.0) and galaxies (stellarity index = 0.0). The commonly used cut-off for this index is 0.8 as taken from the K-band data (e.g. Best et al. 2003). In our survey, we used a stellarity index below 0.8 in J and R to classify an object as a galaxy. Objects which have R magnitudes fainter than the limiting magnitude were counted as objects with no optical detection. The calculated J-band stellarity index was used for the star-galaxy separation for these objects. For example objects classified as a galaxy in J but without a detection in R are classified as a galaxy.

In addition to this automatic selection, we visually examined each ERO candidate to ensure that it is indeed a real detection (i.e. seen in all exposures, not an uncorrected bad pixel, etc.).

At this point we did not correct for extinction. Nevertheless, according to de Vaucouleurs & Buta (1983), and references therein, the Sun is at the common apex of two dust-free cones of ~90° aperture centered at the galactic poles. One of their models for galactic extinction assumes $A \equiv 0$ at all $|b| > 50°$ (polar windows) and assigns a low value at $|b| < 40°$, either $A_B = 0.12(|\cos b| - 1)$ or $A_B = 0.13(|\cos b| - 1)$ (Sandage 1972), with an unspecified smooth transition in the latitude interval $40° < |b| < 50°$. The second approximation was successfully used by Chen et al. (1999) in their 3-dimensional extinction model. Its application to globular and open cluster data indicates that the COBE/IRAS reddening map by Schlegel et al. (1998) has an accuracy of 18% and overestimates visual absorption by a factor of 1.16. This systematic error does not change with galactic latitude.

As a result of the varying exposure times for the R-band data, the fields differ in depth, which is especially important for assigning a colour to objects which have a near-infrared detection but no optical counter-part. This is the case for many EROs. The colour for objects without R-band detection, i.e. $R > R_{\lim}$, was calculated in terms of $R_{\lim} - J$ instead of $R - J$, making the $R - J$ colour a lower limit. The detection limit is obtained from the R_{err} vs. R_{mag} plot (Fig. 4), and corresponds to the maximum R_{mag} for which $R_{err} < 0.1$ mag (R_{err} is the error of the magnitude as given by SExtractor).

3. Results

3.1. The relevance of the $R - J \geq 5$ colour criterion

Most ERO surveys of recent years rely on a colour criterion based on $R - K$, such as $R - K \geq 5$ (Daddi et al. 2000; Roche et al. 2002) or $R - K \geq 6$ (Yan & Thompson 2003). This selects
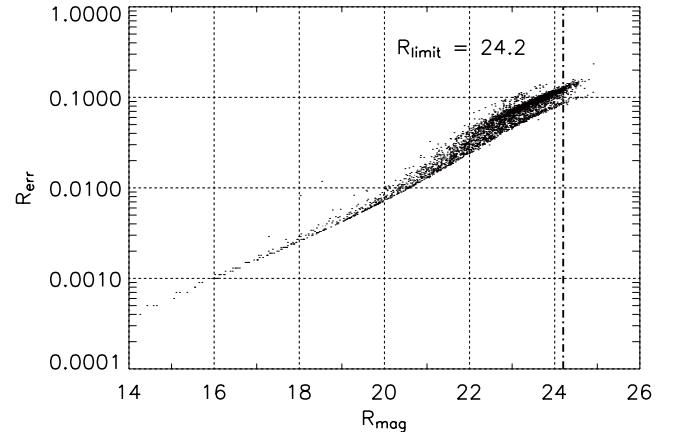

Fig. 4. The R-band detection limit is given by the magnitude at which the majority of photometric errors reach 0.1 mag.

old, passively evolved galaxies as well as starbursts. In order to clarify the colour evolution for various galaxy populations, we used the *Pégase2* code by Fioc & Rocca-Volmerange (1997) to model different formation scenarios. All galaxies were assumed to have formed with a Salpeter IMF and a solar metallicity, but otherwise different parameters. We have investigated 5 scenarios:

(i) elliptical galaxy, formed at $z_f = 10$, with star formation lasting ~200 Myr and an exponential decay time ($\tau \sim 0.1$ Gyr);

(ii) elliptical galaxy with an identical star formation scenario as in (i) but with a formation redshift $z_f = 5$;

(iii) intense and constant star formation of 50 $M_\odot$ yr^{-1} for a galaxy with $M_{gal} = 5 \times 10^{11} M_\odot$ and strong dust reddening ($E(B-V) = 1.0, z_f = 5$);

(iv) disk structure with an edge-on orientation and a constant SFR of 5 $M_\odot$ yr^{-1}, for a galaxy with $M_{gal} = 5 \times 10^{11} M_\odot$, $z_f = 5$;

(v) as in scenario (iv) but with face-on orientation.

The *Pégase2* code allows the inclusion of geometry-dependent extinction. For ellipticals, we used the spheroidal geometry and for spirals, a disk geometry with maximal and minimal inclination. The colours of a galaxy with intense star formation have been reddened to $E(B-V) = 1.0$ by a screen of dust ($R_V = 3.1$).

To simplify matters, all K filters ($K \equiv K' \equiv K_s$) as well R-band filters ($R_C \equiv R_{Johnson}$) were treated as equal.

The left panel in Fig. 5 shows the evolution of $R - J$ colour with redshift for the different galaxy formation scenarios. Our results show that only elliptical galaxies with an already old stellar population, at redshift $z \geq 1.4$, have colours redder than $R - J = 5$. For example, models representing a starburst galaxy or an evolving spiral galaxy do not produce such red ($R - J$) colours. For comparison, panel (b) in Fig. 5 shows the evolution of the $R - K$ colour for the same models. In agreement with previous works (Roche et al. 2002, 2003; Väisänen & Johansson 2004), a sample of galaxies with $R - K \geq 5$ consists of both evolved ellipticals and starburst galaxies.

It is clear that our ERO sample is not comparable with a $R - K \geq 5$ selected sample, since these colour criteria select different ERO populations. However, a small fraction of
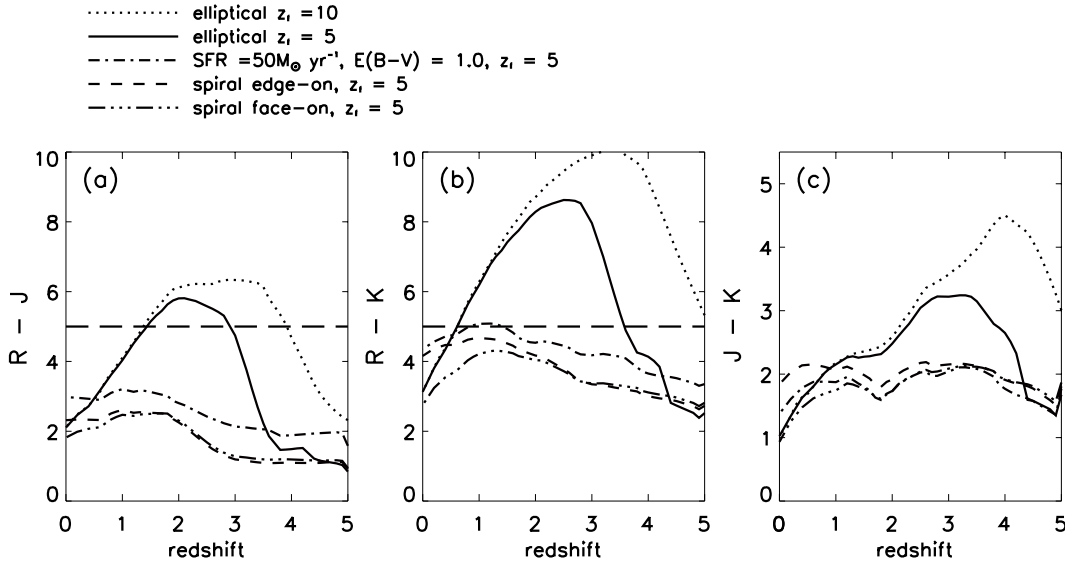
Fig. 5. Colour evolution for different models representing an evolved elliptical galaxy, a dust reddened starburst and a normal spiral galaxy both in an edge-on and face-on orientation. The three panels show the evolution of $R - J$ (panel **a**)), $R - K$ (panel **b**)) and $J - K$ (panel **c**)) colours for all 5 models described in Sect. 3.1. The horizontal dashed line shows the applied colour threshold of our EROs selection $R - J \geq 5$, indicating that we select only ellipticals at redshift 1.4 and above with this colour criteria.

$R - K \geq 5$ selected objects might be as red as $R - K > 7$, which is comparable to $R - J \geq 5$, and our sample can be considered as subset of $R - K$ selected EROs. Therefore, we would expect the surface density of $R - J \geq 5$ selected objects to be smaller than that one for the $R - K \geq 5$ sample.

Any comparison of our results regarding surface density requires an assumption as to the relation between $R - K$ and $R - J$ colours. In addition to the general colour conversion, we have to consider the differences between the various filters, e.g the R-band filter function provided by P*ÉGASE*2 and the filter function for our data set. The obtained colours refer to the specific filters used for our observations. The modeled magnitudes are based on the the transmission function of the R-band filter of the PFCCD (CTIO), the J-band filter of OmegaPrime (Calar Alto) and the K_s filter of ISAAC (VLT).

The right panel of Fig. 5 shows the evolution of $J - K$ colour, suggesting that an old elliptical galaxy with $R - J \geq 5$ and redshift $z \sim 1.4$ would have $J - K \geq 2.25$. This is consistent with the results of van Dokkum et al. (2003), who found galaxies with $J_s - K_s = 2.35$ and redshifts of $z > 1.2$ (~17% of the sample) and $z > 2.3$ respectively. Finding such an elliptical galaxy at even higher redshift requires a $J - K$ colour around 3 (for $z_f = 5$) and higher (for $z_f = 10$), according to our models. Objects with such red near-infrared colours are named Hyper Extremely Red Objects (HEROs), and are thought to be dusty star-forming objects at $z \geq 2$ or old galaxies at $z \sim 2$–3 (Im et al. 2002b, and references therein). The combination of our models and the properties of HEROs support the assumption that objects with $R - J \geq 5$ are indeed elliptical galaxies with redshift ~1.5–3.0 (for $z_f = 5$).

Compared to the results of Yan & Thompson (2003), our $J - K$ colour for evolved ellipticals at redshift 1.5 and $R - J \geq 5$ is about 0.25 mag bluer, which might be the result of

either different evolutionary scenarios or slightly different filter functions.

3.2. The J-band galaxy counts

The number of J-band surveys is relatively small and lacks sky coverage. Bershady et al. (1998) and Saracco et al. (1999) have published deep J-band counts; other surveys extend the magnitude range to $13 < J < 20$, e.g. MUNICS (Drory et al. 2001) and Väisänen et al. (2000). Our survey covers a similar magnitude range, but a 4 times larger area. However, the number counts shown in Fig. 6 agree well with the number counts of Drory et al. (2001) and Väisänen et al. (2000), although they are somewhat higher than the Saracco et al. (1999) and Martini (2001) counts.

The Sarraco et al. (1999) survey extends to much fainter galaxies than does ours, and the two surveys overlap only at our faintest magnitudes. In this range, the calculated surface density is affected by the small number statistics. All the J-band counts in the range 13–18 mag have essentially the same slope as our data, $\alpha \approx 0.53$. Also the flattening at the faint end agrees with the result of Saracco et al. (1999), who found slopes of ≈0.35 and 0.34, respectively.

The observed differences can be partially explained by different definitions of the J magnitude, e.g. IRAF aperture magnitude or SExtractor magnitude.

3.3. ERO sample

Figure 7 shows the distribution of colours for all galaxies (in both bands) between $15 \leq J \leq 20$, from which the mean $R - J$ colour and *FWHM* in different J magnitude intervals have been calculated (see Table 2). The mean colour in the intervals up to $J < 20$ increases by 1.17 mag from $R - J = 1.68$

Table 2. $R - J$ colour distribution. The two values represent the total number of EROs in the specified magnitude interval and the fraction which has an optical counterpart.

J-magnitude	mean $R - J$ colour	$FWHM$	EROs
$14 \leq J < 15$	1.68 ± 0.01	0.388 ± 0.008	0
$15 \leq J < 16$	1.73 ± 0.01	0.473 ± 0.014	0
$16 \leq J < 17$	1.79 ± 0.01	0.544 ± 0.024	1/1
$17 \leq J < 18$	1.86 ± 0.04	0.837 ± 0.090	9/9
$18 \leq J < 19$	3.08 ± 0.02	1.679 ± 0.020	41/21
	5.16 ± 0.06	0.637 ± 0.066	
$19 \leq J < 20$	2.85 ± 0.03	1.489 ± 0.028	9/4
	4.30 ± 0.00 (fixed)	1.656 ± 0.127	
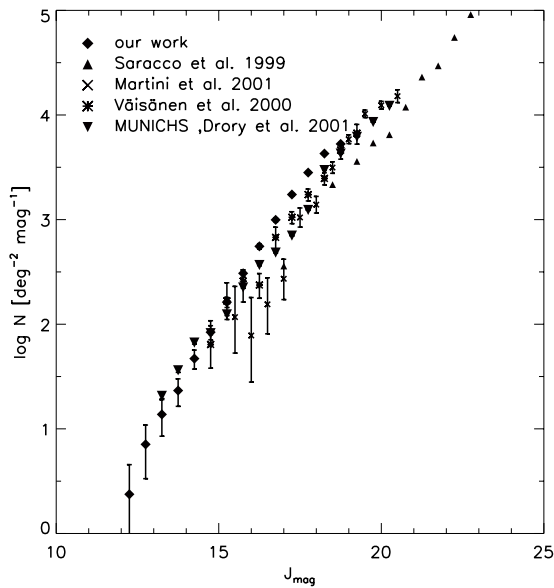
Fig. 6. Differential counts (number mag^{-1} deg^{-2}) of galaxies in the J-band compared to a collection of published data, including Saracco et al. (1999), Martini (2001), Väisänen et al. (2000) and the MUNICS survey (Drory et al. 2001). The error bars for our data represent only counting statistics.

to $R - J = 2.85$. Such a trend was also observed by Daddi et al. (2000) and Thompson et al. (1999) for the mean $R - K$ colours, which reach their maximum between $K \sim 18-19$. This reddening of the mean colour might result from a growing fraction of high-redshift galaxies.

The EROs satisfying our colour criterion lie in a range $17 \leq J \leq 20$, and appear to build a second population of galaxies. Such an additional peak has never been observed before and therefore requires clarification. Follow-up analysis shows this feature to be the result of the R-band detection limit. About 42 percent of these EROs have no R-band detection. Therefore, the limiting R-band magnitude for each separate field has been used as substitute. As a result the $R - J$ colour of those objects is an estimate for the lower limit. The second peak, therefore, is an artefact of assigning the limiting R magnitude to non-detections.

Column 4 in Table 2 lists number of visually confirmed EROs and number of EROs with R-band detection. In total, we found 35 objects with $R - J \geq 5$, which have a stellarity index

of 0.8 in both bands. An additional 25 objects have no R-band detection but their J-band stellarity classifies them as galaxy. Examples of both classes appear in Fig. 8. The limited spatial resolution in R and J permits no discrimination between the different morphological galaxy types. However, their appearance will be useful for the selection of objects for follow-up observations.

Figure 9 shows the colour–magnitude diagram for these 79 extremely red objects, including both stars (19) and galaxies (60). We also differentiate between objects which are stars or galaxies in both bands or in the J-band alone. Although we used the stellarity index as a criterion to distinguish between stars and galaxies, the number of galaxies with no R-band detection has to be treated as an upper limit. Deeper optical photometry might identify these as stars.

3.4. Surface density

In an area of 2.89 degree^2 we found 60 EROs (classified as galaxies), yielding a surface density of $(5.75 \pm 0.74) \times 10^{-3}$ arcmin^{-2} (Poisson uncertainties). Counting only objects which have both optical and near-infrared detection, this number decreases to 35, dropping the surface density to $(3.36 \pm 0.56) \times 10^{-3}$ arcmin^{-2}. Figure 10 shows our result in comparison to the only other survey selecting EROs with an extreme colour threshold, the $R - K \geq 7$ selection from Daddi et al. (2000). For comparison, we have adopted a colour relation of $J - K = 2.3$ based on the stellar population models.

Daddi found 5 such objects within the completeness limit of their deep survey ($K \leq 19.2$, area = 447 arcmin^2). Keeping in mind that the Daddi et al. sample has fainter near-infrared magnitudes, the resulting surface density of 0.011 arcmin^{-2} is larger than our result by a factor of 1.9. This difference increases by another factor of 2 if we count only objects with R-band detection. Deeper follow-up observations, e.g. with ISAAC and FORS, will constrain the surface density further.

The large variations in the spatial distribution, and the high density of EROs in single fields, suggest that EROs are clustered. Figure 11 shows the distribution of all 60 extremely red galaxies found in all 50 survey fields. In approximately one third of the fields, no ERO was detected, while 4 fields contain 4 EROs yielding a surface density of 0.0192 arcmin^{-2}, more than three times the the average surface density of the whole sample.

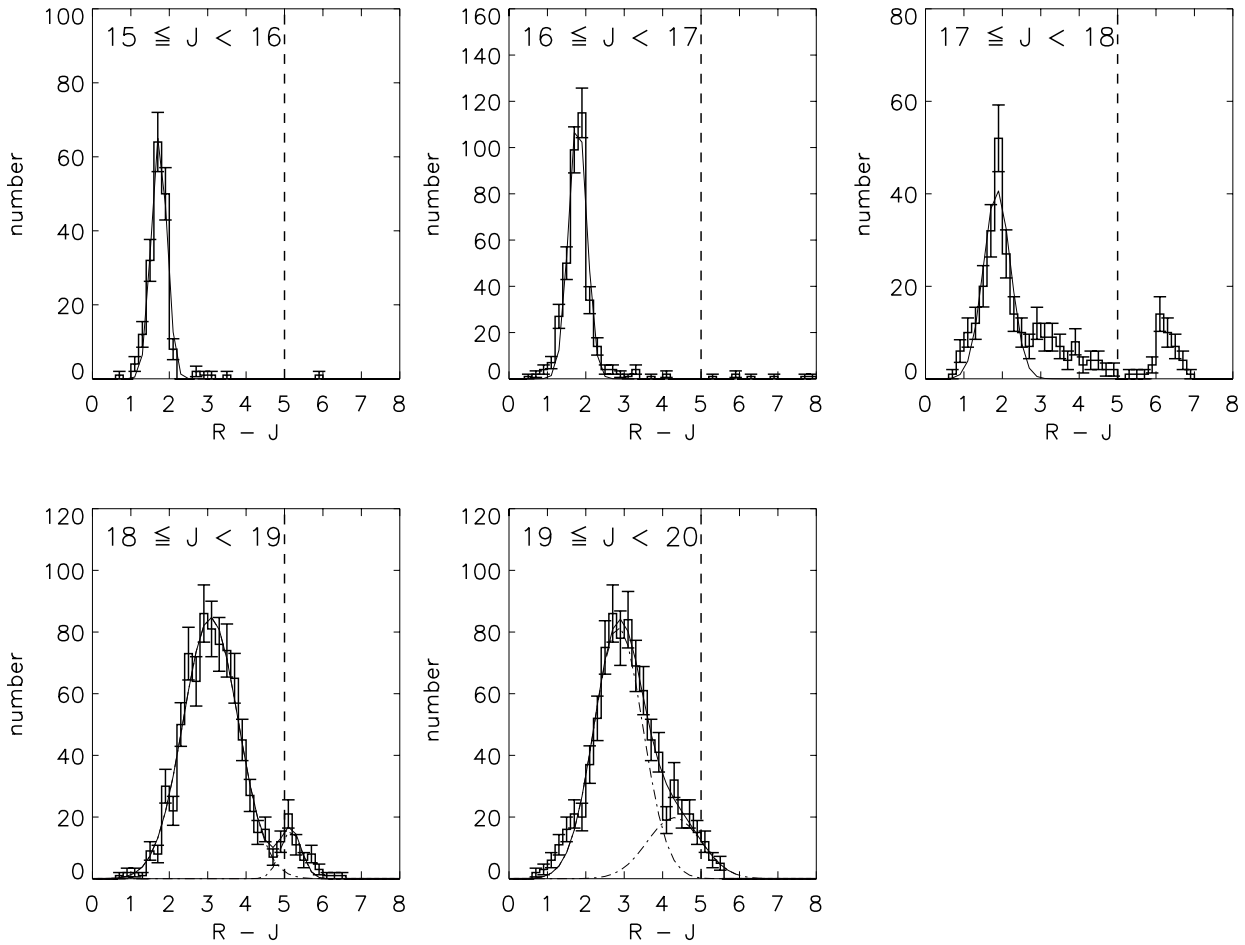**Fig. 7.** $R - J$ colour distribution for all galaxies, i.e. stellarity index ≤0.8 in R and J-band. Magnitude ranges are indicated in the upper left-hand corner of each panel. The data show the colour distributions without visual check (as was done for the final catalogue of extremely red objects, $R - J \geq 5$), i.e. objects to the left of the dashed line were not manually checked in each individual frame. The error bars indicate the Poisson uncertainties and the dot-dashed lines show the one or two Gaussians used to fit the peak position and width of the distribution reported in Table 2. The second peak is the result of assigning the limiting R magnitude to objects with no optical detection (see text for details).
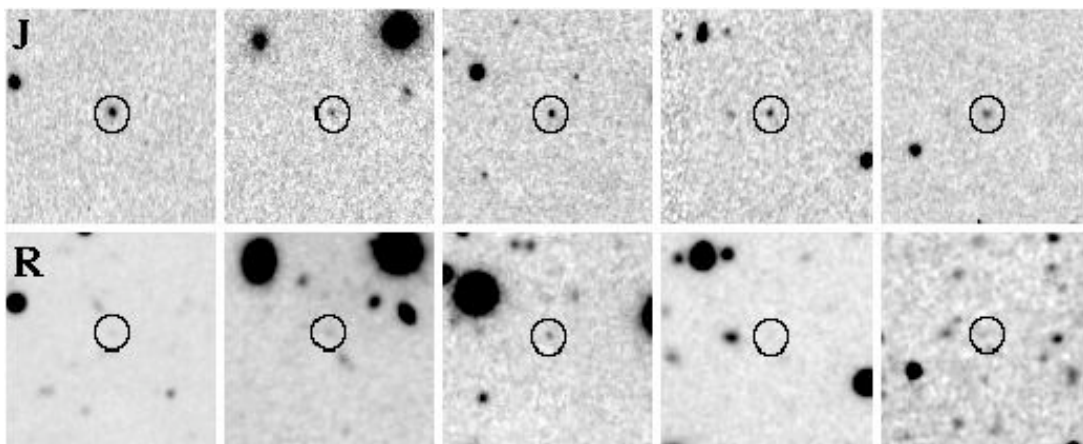

Fig. 8. Examples of EROs, with R-band detection (*leftmost three panels*) and without optical detection (*rightmost two panels*). The images are 40″ on a side.

However, the small number of $R - J \geq 5$ galaxies in each field prevents the calculation of clustering amplitudes. Deeper follow-up observations on selected fields which contain a larger than average number of EROs may also find fainter or less red members of a galaxy cluster.

3.5. Volume density

Although we have no redshift information for our sample, we can make a crude estimate of the volume density of EROs, based on the redshift range in which such objects can occur.
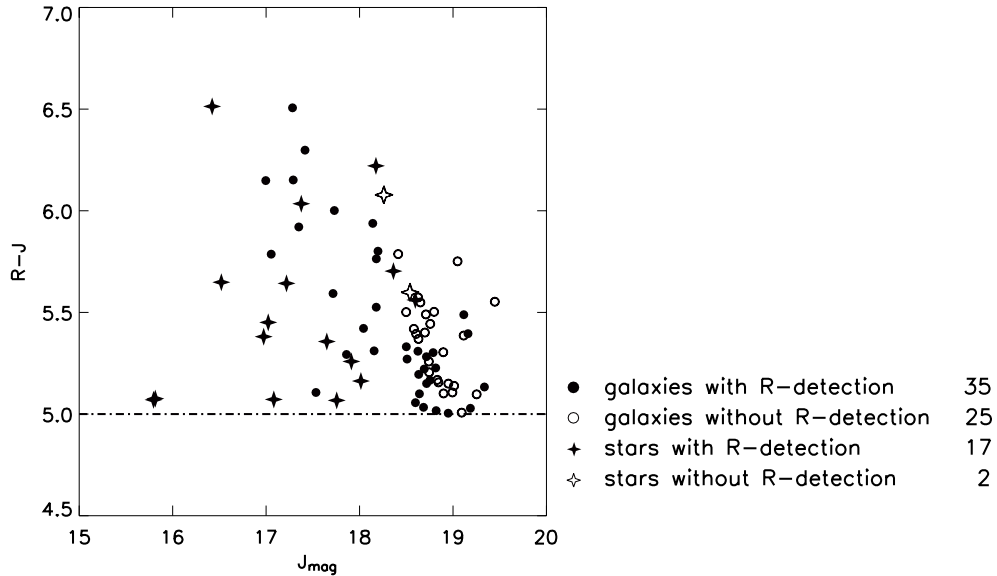
Fig. 9. Colour–magnitude diagram for extremely red stellar objects (19) and galaxies (60) found in our survey. For objects without R detection, the star/galaxy classification in R is arbitrary and solely based on the SExtractor result, the dashed line marks the $R - J \geq 5$ colour threshold.
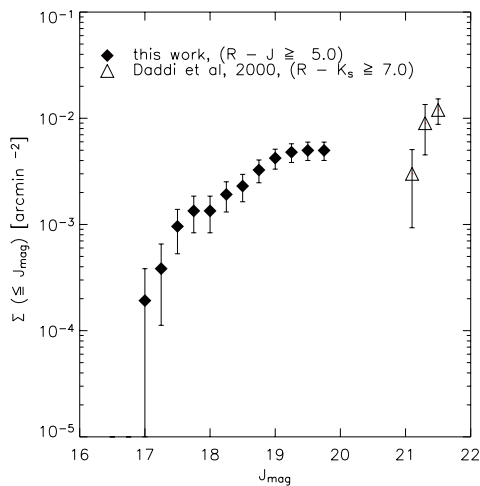

Fig. 10. Cumulative ERO surface density from this work, compared to the results for $R - K \geq 7$ objects from Daddi et al. (2000). The uncertainties are derived assuming only Poisson counting statistics. To convert the Daddi K-band magnitudes into J-band we use the result of the stellar population synthesis models, which found a $J - K = 2.25$ for objects with $R - J \geq 5$ (Fig. 5).

Fig. 11. Number distribution of the 60 extremely red galaxies found in 50 survey fields.

The very red optical to near-infrared colour of an elliptical galaxy is the result of a strong 4000 Å break, shifted between the R- and J-bands. For elliptical galaxies with $R - J \geq 5$ the SSP model (model ii in Sect. 3.1) predicts a redshift range $1.4 \lesssim z \lesssim 3.0$, for which this colour criteria is satisfied.

The co-moving volume covered in this range, accumulated over all 50 fields in the assumed cosmology is 6.3×10^6 Mpc^3. For our sample of 60 EROs, this yields a volume density of $(9.57 \pm 1.23) \times 10^{-6}$ Mpc^{-3}. The error reflects only the low number statistics, and not the uncertainty in the volume estimate. EROs with a generally bluer cutoff, $R - K \geq 6$, have a volume density which is approximately twice the volume density
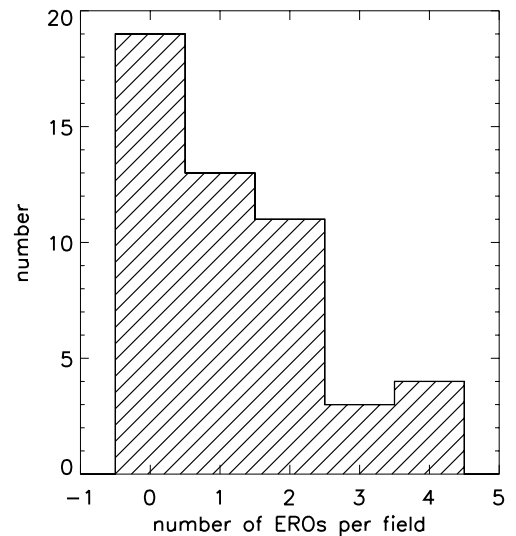
of our sample, averaged over a redshift range of $0.85 \leq z \leq 2$ (Thompson et al. 1999).

This space density is approximately four times higher than that for other bright objects, e.g. quasars. Boyle et al. (2000) found a space density of 2×10^{-6} Mpc^{-3} for quasars with $M_B \leq -23$ in a similar redshift range. The comparatively large volume density at higher redshifts suggests that massive structures have been formed early in the universe.

4. Summary

In order to study the properties of galaxies with $R - J \geq 5$, we have constructed a sample of EROs from R and J-band photometry of a total of a 2.89 deg^2 area of sky.

Taking into account the varying 10σ detection limits in the J-band ($\sim 19.5^{\mathrm{mag}}$), we are looking at an extremely bright, i.e.

very massive galaxy population. Stellar evolution models indicate that these galaxies to lie in a redshift range between 1.4 and 3.0.

We have detected 60 EROs, 35 of which have both J and R-band (10σ) detections. The total sample of EROs has a surface density of $(5.75 \pm 0.74) \times 10^{-3}$ arcmin^{-2}, leading to a volume density of $(9.57 \pm 1.23) \times 10^{-6}$ Mpc^{-3}, assuming a model-dependent redshift.

This sample, being bright, lends itself well to spectroscopic follow-up observations, which will allow both the determination of the redshift and a clear classification as a distinct ERO population.

References

Afonso, J., Mobasher, B., Chan, B., & Cram, L. 2001, ApJ, 559, L101
Alexander, D. M., Vignali, C., Bauer, F. E., et al. 2002, AJ, 123, 1149
Bell, E. F., Wolf, C., Meisenheimer, K., et al. 2004, ApJ, 608, 752
Bershady, M. A., Lowenthal, J. D., & Koo, D. C. 1998, ApJ, 505, 50
Bertin, E., & Arnouts, S. 1996, A&AS, 117, 393
Best, P. N., Lehnert, M. D., Miley, G. K., & Röttgering, H. J. A. 2003, MNRAS, 343, 1
Bizenberger, P., McCaughrean, M. J., Birk, C., Thompson, D., & Storz, C. 1998, in Infrared Astronomical Instrumentation, ed. A. M. Fowler, Proc. SPIE, 3354, 825
Boyle, B. J., Shanks, T., Croom, S. M., et al. 2000, MNRAS, 317, 1014
Brusa, M. 2003, Astron. Nachrichten, 324, 113
Brusa, M., Comastri, A., Daddi, E., et al. 2002, ApJ, 581, L89
Cimatti, A., Daddi, E., di Serego Alighieri, S., et al. 1999, A&A, 352, L45
Cimatti, A., Daddi, E., Mignoli, M., et al. 2002a, A&A, 381, L68
Cimatti, A., Pozzetti, L., Mignoli, M., et al. 2002b, A&A, 391, L1
Cowie, L. L., Gardner, J. P., Hu, E. M., et al. 1994, ApJ, 434, 114
Daddi, E., Cimatti, A., Pozzetti, L., et al. 2000, A&A, 361, 535
Daddi, E., Cimatti, A., Broadhurst, T., et al. 2002, A&A, 384, L1
de Vaucouleurs, G., & Buta, R. 1983, AJ, 88, 939
Drory, N., Feulner, G., Bender, R., et al. 2001, MNRAS, 325, 550
Elston, R., Rieke, G. H., & Rieke, M. J. 1988, ApJ, 331, L77
Elston, R., Rieke, M. J., & Rieke, G. H. 1989, ApJ, 341, 80
Firth, A. E., Somerville, R. S., McMahon, R. G., et al. 2002, MNRAS, 332, 617
Frayer, D. T., Reddy, N. A., Armus, L., et al. 2004, AJ, 127, 728
Gilbank, D. G., Smail, I., Ivison, R. J., & Packham, C. 2003, MNRAS, 346, 1125
Graham, J. R., & Dey, A. 1996, ApJ, 471, 720
Hall, P. B., Sawicki, M., Martini, P., et al. 2001, AJ, 121, 1840
Hempel, A., Herbst, T. M., & Thompson, D. 2003, Ap&SS, 285, P33
Herbst, T. M., Thompson, D., Fockenbrock, R., Rix, H.-W., & Beckwith, S. V. W. 1999, ApJ, 526, L17
Hu, E. M., & Ridgway, S. E. 1994, AJ, 107, 1303
Im, M., Simard, L., Faber, S. M., et al. 2002a, ApJ, 571, 136
Im, M., Yamada, T., Tanaka, I., & Kajisawa, M. 2002b, ApJ, 578, L19
Liu, M. C., Dey, A., Graham, J. R., et al. 2000, AJ, 119, 2556
Mannucci, F., Pozzetti, L., Thompson, D., et al. 2002, MNRAS, 329, L57
Martini, P. 2001, AJ, 121, 2301
McCracken, H. J., Metcalfe, N., Shanks, T., et al. 2000, MNRAS, 311, 707
Mohan, N. R., Cimatti, A., Röttgering, H. J. A., et al. 2002, A&A, 383, 440
Moriondo, G., Cimatti, A., & Daddi, E. 2000, A&A, 364, 26
Moustakas, L. A., Casertano, S., Conselice, C. J., et al. 2004, ApJ, 600, L131
Pozzetti, L., & Mannucci, F. 2000, MNRAS, 317, L17
Roche, N. D., Almaini, O., Dunlop, J., Ivison, R. J., & Willott, C. J. 2002, MNRAS, 337, 1282
Roche, N. D., Dunlop, J., & Almaini, O. 2003, MNRAS, 346, 803
Sandage, A. 1972, ApJ, 178, 1
Saracco, P., D'Odorico, S., Moorwood, A., et al. 1999, A&A, 349, 751
Schmidt, B. P., Suntzeff, N. B., Phillips, M. M., et al. 1998, ApJ, 507, 46
Smail, I., Ivison, R. J., Kneib, J.-P., et al. 1999, MNRAS, 308, 1061
Smith, G. P., Treu, T., Ellis, R., et al. 2001, ApJ, 562, 635
Smith, G. P., Smail, I., Kneib, J.-P., et al. 2002a, MNRAS, 333, L16
Smith, J. A., Tucker, D. L., Kent, S., et al. 2002b, AJ, 123, 2121
Soifer, B. T., Matthews, K., Neugebauer, G., et al. 1999, AJ, 118, 2065
Somerville, R. S., Primack, J. R., & Faber, S. M. 2001, MNRAS, 320, 504
Thompson, D., Beckwith, S. V. W., Fockenbrock, R., et al. 1999, ApJ, 523, 100
Väisänen, P., & Johansson, P. H. 2004, A&A, 421, 821
Väisänen, P., Tollestrup, E. V., Willner, S. P., & Cohen, M. 2000, ApJ, 540, 593
van Dokkum, P. G., Förster Schreiber, N. M., Franx, M., et al. 2003, ApJ, 587, L83
Wehner, E. H., Barger, A. J., & Kneib, J.-P. 2002, ApJ, 577, L83
Yan, L., McCarthy, P. J., Weymann, R. J., et al. 2000, AJ, 120, 575
Yan, L., & Thompson, D. 2003, ApJ, 586, 765
Yan, L., Thompson, D., & Soifer, B. T. 2004, AJ, 127, 1274